Scanning Capacitance Characterization of Potential Screening in InAs Nanowire Devices

James J. M. Law,[†] *Student Member, IEEE*, Shadi A. Dayeh,[†] *Student Member, IEEE*, Deli Wang,[†] *Member, IEEE,* and Edward. T. Yu,[†,*] *Member, IEEE*
[†]Department of Electrical and Computer Engineering
University of California, San Diego
9500 Gilman Dr., La Jolla, CA 92093-0407
*E-mail: ety@ece.ucsd.edu

***Abstract*-We have used scanning capacitance microscopy (SCM) and spectroscopy (SCS) to examine the effects of micron-scale metal contacts, typically present in nanowire-based electronic devices, on carrier modulation and electrostatic behavior in InAs semiconductor nanowires. We observe a pronounced dependence of scanning capacitance images and spectra on distance between the scanning capacitance probe tip and nanowire contact up to distances of 3-4 μm. Based on comparison of these data with results of finite-element electromagnetic simulations, we interpret these results as a consequence of electrostatic screening of the tip-nanowire potential difference by the large metal contact. The results provide direct experimental verification of contact screening effects predicted in the literature, and are expected to have substantial implications for the design and expected performance of nanowire-based electronic devices, most notably nanowire field-effect transistors. Ultimately, they are indicative of the importance of assessing and accounting for the effect of large-scale contact and circuit elements on the characteristics of nanoscale electronic devices.**

I. Introduction

Semiconductor nanowires offer promising capabilities for future high-performance electronic [1], optoelectronic [2], biomedical [3], and thermoelectric [4] devices and new platforms for basic investigations of electronic structure and carrier transport in low-dimensional systems. InAs nanowires, in particular, are a superb candidate for high speed, high density, ultra-low power circuits due to their narrow band gap (0.354 eV), high electron mobility–in excess of 33,000 cm^2/Vs in bulk material–and surface Fermi-level pinning in the conduction band, which allows for formation of ohmic contacts with relative ease. Because of the new geometries often employed in nanowire-based devices, understanding the interaction and influence of nearby macro-scale objects, such as bulk contacts, on nanowire behavior is of paramount importance.

II. Experiment

We have used scanning capacitance microscopy (SCM) and spectroscopy (SCS)–confirmed with finite-element numerical simulations–to examine the effects of micron-scale metal contacts typically present in nanowire-based electronic devices on carrier modulation and electrostatic behavior in semiconductor nanowires. Unintentionally doped *n*-type InAs

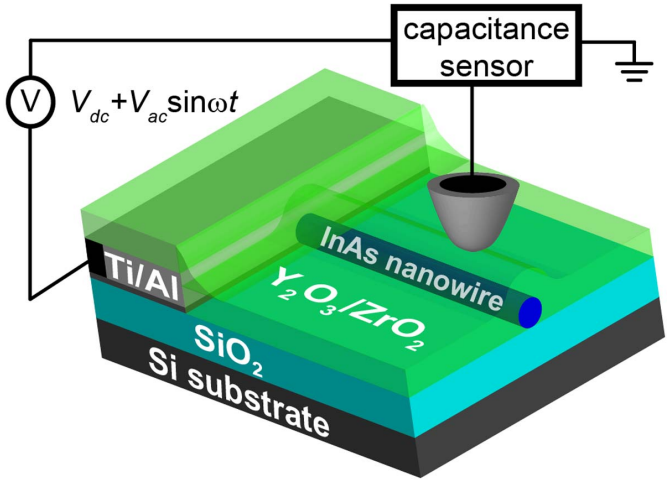

Fig. 1. Schematic diagram of sample structure, scanning probe measurement geometry, and voltage biasing arrangement.

semiconductor nanowires with diameters of 70 – 115 nm were grown by metalorganic chemical vapor deposition [5] using colloidal Au nanoparticles as catalysts on thermally oxidized Si substrates. Electrical device structures were fabricated by sonication of nanowires into an ethanol solution and deposition of the nanowires onto a thermally oxidized Si wafer, followed by metallization and ohmic contact formation to single nanowires using electron-beam lithography and electron-beam evaporation of 2 μm-wide metal strips [6]. Finally, a 73 nm Y_2O_3/ZrO_2 film (relative dielectric constant ~ 12) was sputter deposited to act as the insulating layer between the probe tip and the nanowire surface. Top-gated current-voltage measurements of wires fabricated in an identical fashion were carried out to verify the ohmic nature of the contacts and extract important device parameters such as mobility and carrier concentration. A Digital Instruments (Veeco) Nanoscope IIIa Dimensions 3100 microscope with a diamond-coated probe tip was utilized to probe the nanowire capacitance versus voltage characteristics near a single contact, yielding both scanning capacitance images at fixed bias voltages, and local spectra of the scanning capacitance signal, dC/dV, as a function of bias voltage. For SCM measurements, a bias voltage consisting of a dc component with small (~2 V) ac modulation, typically at a frequency of 20-95 kHz, was applied to the sample with the probe tip grounded. For SCS

978-1-4244-2104-6/08/$25.00 ©2008 IEEE.

measurements, the probe tip was held in a constant position while a low frequency (~0.5 Hz), saw-tooth wave of varying amplitude between 6 and 12 V and a high frequency (20-95 kHz) and ~ 2 V sine-wave bias were applied to the sample with the probe tip grounded. As discussed in detail elsewhere [7]-[9], the SCM/SCS signal detection mechanism yields a voltage signal that is proportional, in our measurements, to *dC/dV*, where *C* is the tip-sample capacitance and *V* is the dc component of the applied bias voltage. Typical ambient conditions for these experiments were ~20 ˚C and ~ 50% relative humidity. For ease of interpretation in terms of analogous behavior of a conventional metal-insulator

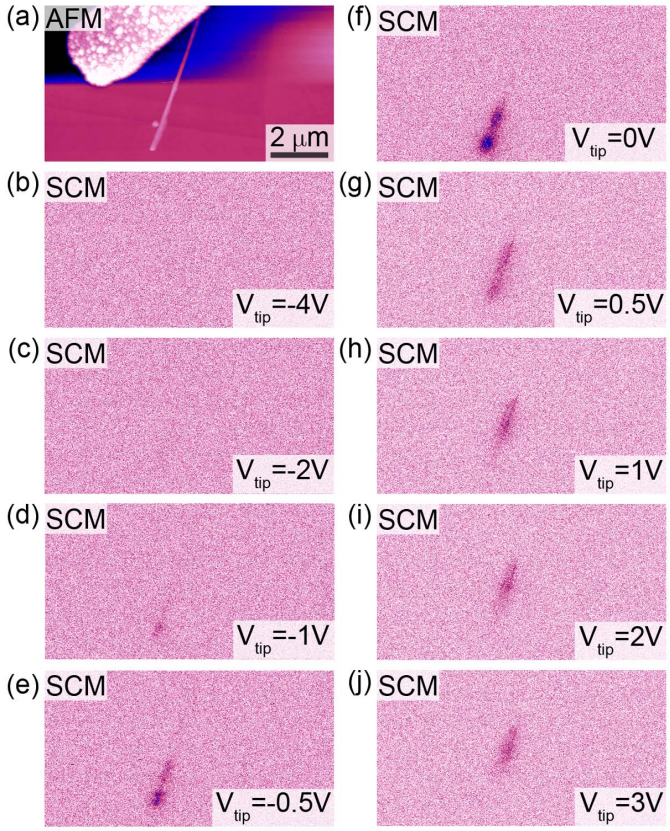

Fig. 2. (a) AFM topograph and (b)-(j) SCM images obtained at dc bias voltages of -4V, -2V, -1V, -0.5V, 0V, 0.5V, 1V, 2V, and 3V, respectively.

semiconductor structure, for which it is typical to specify the voltage applied to the metal contact relative to the semiconductor, we at this point adopt the convention of specifying the potential of the probe tip relative to the sample in discussion and analysis of the SCM/SCS data. Fig. 1 shows a schematic diagram of the sample and probe tip geometry employed in these experiments.

Finite element electrostatic simulations were carried out using the commercial simulation package COMSOL Multiphysics. The simulation geometry sought to mimic the electrostatic environment in the experimental geometry as accurately as possible. Thus, a wire of 7 μm in length and 70 nm in diameter; a rectangular metallic contact of 7 μm in length, 3 μm in width, and 70 nm in height; and a probe with tip radius of curvature of 50 nm and a conical cross section of 7μm in height and 3.5 μm in radius at the base were created. The wire and the contact were both conformally coated in a dielectric layer of 73 nm in thickness and with relative dielectric constant ε_r = 12. Further simulations were carried out with a smaller contact measuring 200 nm in length, 3 μm in width, and 70 nm in height in order reduce the cross-sectional area normal to the long axis of the wire. The wire was given a dielectric constant of bulk InAs (ε_r = 15) and an electrical conductivity of 6×10^4 S/m, which was calculated from current-voltage characteristics on the wires in this experiment. Both the contact and the probe tip were treated as equipotential surfaces at two volts and ground, respectively. The probe tip was placed at the apex of the wire/dielectric system and at regular intervals along the axial direction of the wire, as schematically illustrated in Fig. 1. The simulation yielded the potential profile of the entire simulated geometry.

III. RESULTS & DISCUSSION

Fig. 2(a) shows an AFM topograph of a nanowire and contact. Figs. 2(b)-(j) show SCM images of the same area corresponding to the topographic image in Fig. 2(a), obtained at dc bias voltages of -4 V to +3 V applied to the tip relative to the grounded sample. Figs. 2(b) and (c) show no SCM contrast indicating that at these dc biases the *dC/dV* curve is flat. With the increase of the dc bias to -1 V, as in Fig. 2(d), we begin to see a small amount of SCM contrast. At -0.5 V and 0 V, as in Figs. 2(e) and (f), the contrast level has increased dramatically. In Figs. 2(g)-(i), the contrast begins to decrease, but the center

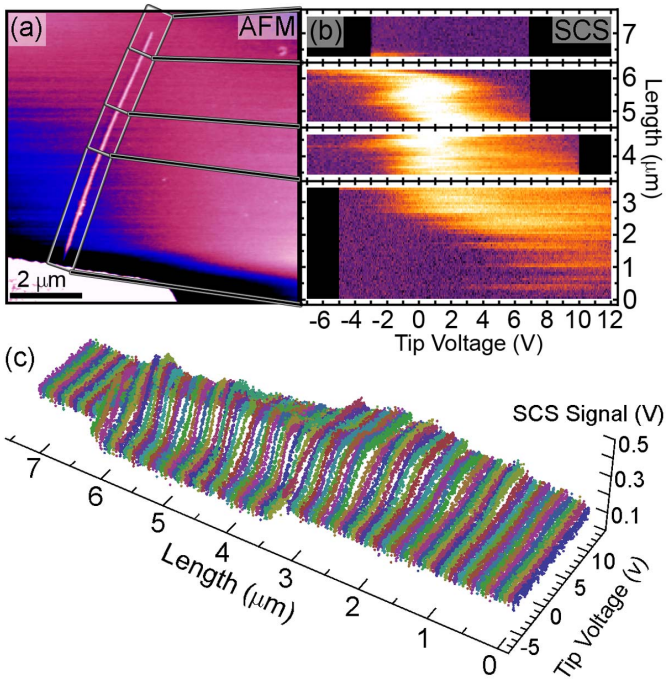

Fig. 3. (a) AFM topograph, (b) Density plot of SCM signal versus length along the nanowire, and (c) individual line slices of SCM data as a function of tip voltage and length along the nanowire where the black regions indicate not data collected.

of the contrast area begins to move up towards the contact. More generally, as the dc voltage is increased from -4 V to +3 V, the peak of the SCM signal contrast shifts closer to the metal contact. This results indicates that there is an additional influence on the device, for in a semiconductor nanowire (or planar device structure) of uniform doping and potential profile (i.e. no current flow), *C(V)* and thus, *dC/dV,* should be invariant as a function of position, resulting in an SCM image of the nanowire that shows constant signal contrast across the entirety of the sample.

Fig. 3(a) shows an AFM topograph of a wire nearly perpendicular to the contact. The wire is approximately 6.5 μm in length and slightly tapered. Fig. 3(b) shows a density plot of the scanning capacitance spectra versus distance along the wire. Fig. 3(b) consists of four separate plots. The data were collected for the top-most to the bottom-most in four separate dc voltage ranges: -3 V to 7 V; -7 V to 7 V; -7 V to 10 V; and -5 V to 12 V, respectively. The topographic region that corresponds to each of these sections is marked by boxes in Fig. 3(a). Some portions of the top- and bottom-most density plots correspond to areas where there is no wire as seen in the corresponding boxed regions of Fig 3(a). The black portions of Fig 3(b) indicate voltage ranges where no data was collected. It is evident from the density plot that the *dC/dV* versus *V* behavior of the wire is not uniform along the length of the wire. Near the contact, the data show that the peak of the SCS signal is decreasing in value and shifting towards increasingly higher voltages. There also appears to be a slight spreading of the curves. Several microns away from the contact, the SCM signal contrast is larger and does not change as readily as a function of increased distance from the contact.

Fig. 3(c) plots the scanning capacitance signal versus tip voltage and distance from the contact. From this figure, it is easy to see that the peak of the *dC/dV* versus *V* spectra shifts to larger positive voltages as the tip approaches the contact. Each of the *dC/dV* spectra was fitted using a polynomial and subsequently differentiated to find the coordinates of each of the peaks. The abscissa-coordinate of each of the maxima was then plotted versus the tip distance from the contact as in Fig. 4 (a). Spectra taken less than one micron away from the contact had peaks at voltages larger than the detection limit of our instrument (12 V, in this case), as can be seen in Fig. 3 (c), thus they are not included in Fig. 4 (a). Some of the spectra that were towards the non-contacted end of the nanowire had peaks that were too small to definitively extract a peak, thus these values were also not included. Fig. 4 (a) explicitly demonstrates that the spectra-maxima, and thus the threshold voltage, shift in a highly non-linear to exponential fashion as a function of length from the contact. In the experimental geometry, the metal contact is taller than the wire itself by a significant amount, and as a result, the sputter-coated oxide near the contact-nanowire interface has a shape that is a superposition of both the contact and the nanowire. More specifically, the oxide coating is thicker than 73 nm on the top of the wire in proximity to the contact. The increasing thickness of the oxide near the contact changes the electrostatics in this region. Examination of the tip-sample

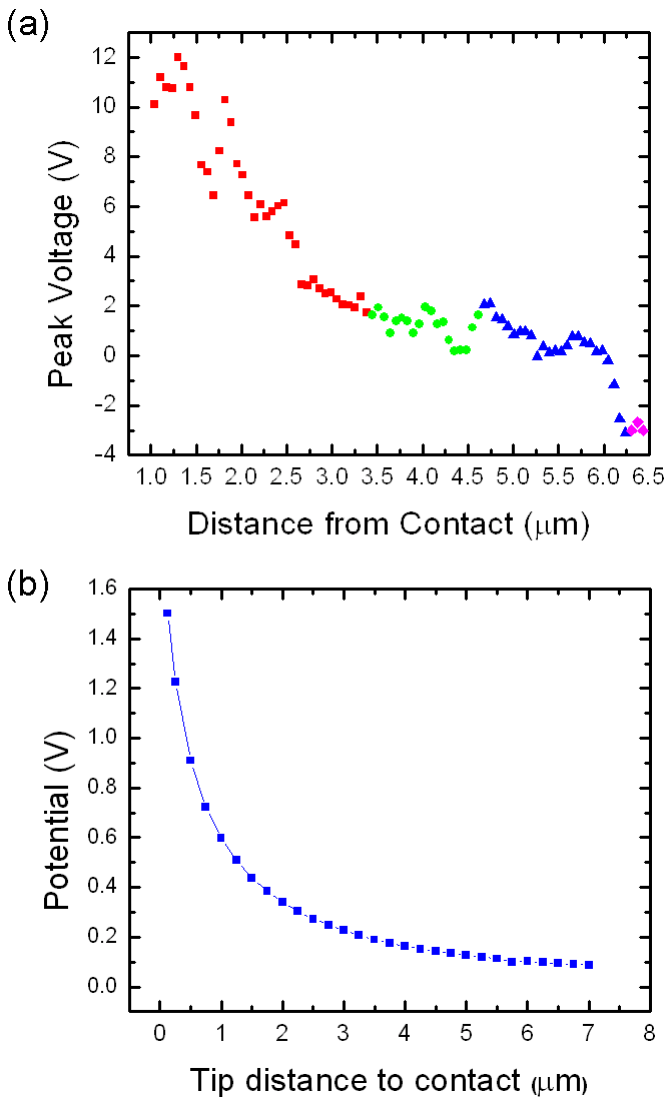

Fig. 4. (a) Plot of the voltage of the peak of the *dC/*dV curve versus the tip distance from the contact with different shapes corresponding to the different sections in Figs. 3 (a) and (b) and (b) plot of the simulated potential at the apex of the wire beneath the probe tip for variable tip-contact separations.

capacitance behavior as a function of distance between the probe tip and a nearby large-area contact reveals the major influence of the large contact on the local electrostatic behavior of the nanowire. Local, nanoscale carrier modulation characteristics and electrostatic behavior of the nanowire vary substantially as a function of distance from the nanowire/contact interface. Specifically, the threshold voltage for carrier accumulation at the InAs surface shifts to lower voltages as the distance from the contact increases, indicating that the large contact screens a significant portion of the electric field from the scanning probe tip even at distances from the contact as large as a few micrometers. An approximately exponential dependence of the screened potential on contact-tip spacing is observed. Increased thickness of the oxide near the contact, as mentioned above, changes the amount of screening by the large contact and may

explain why the data near 1 μm appear to not follow an exponential behavior.

Fig. 4 (b) shows the results of finite-element electromagnetic simulations of the tip-sample experimental geometry. For each point in Fig. 4 (b), a separate simulation was carried out. Each simulation placed the tip at a different distance from the contact. The tip potential was kept at 0 V and the contact at 2 V. The simulation generated the potential profile for the entire structure, and Fig 4 (b) plots the potential directly beneath the tip at the interface between the wire and the oxide for each of the simulated tip-contact separations. Although the potential on the probe tip is always zero, the potential seen on the wire surface is often much larger. Nominally there should be a voltage drop across the oxide which will never allow the potential at the wire-oxide interface to reach zero; however, it is unexpected that this voltage drop should be as large as it is, especially in the case of small distances between the tip and the contact. Fig. 4 (b) confirms that a dramatic electrostatic screening effect is present, and that there is an exponential increase in the amount of electrostatic screening as the probe tip is moved closer to the large metallic contact. Additional simulations on a smaller contact geometry show the decay length of the exponential screening effect can be significantly reduced with a nano-sized metallic source contact. On the basis of the simulated work, we hypothesize that the geometry of the contacts has a dramatic influence on the amount of screening present in the device. A reduction not in contact volume necessarily, but in the relative cross-sectional area facing the nanowire should reduce the amount of coupling that the large contact has on the device. Also, this situation is not meant to exactly mimic the electrostatics of a nanowire field effect transistor, as the AFM tip does not serve as a good conformal contact to the wire. The screening should be significantly reduced with a change in the gate geometry as well as a change in the source/drain geometry. Ref. [10] has demonstrated a reduction in the parasitic effects of source/drain field coupling to the nanowire using silicided Group IV nanowires. Though these results have been predicted before theoretically [11], they have never been directly measured or categorized. These observations could have substantial implications for the design and expected performance of nanowire-based electronic devices, most notably nanowire field-effect transistors (this is true particularly in situations where scanning probes are used to extract device parameters), and are indicative of the importance of assessing and accounting for the effect of large-scale contact and circuit elements on the characteristics of nanoscale electronic devices.

IV. Conclusions

In summary, we have used atomic force microscopy, scanning capacitance microscopy, scanning capacitance spectroscopy, and finite element electrostatic simulations to establish that micron-sized contacts to InAs nanowire devices induce the presence of strong electrostatic potential screening and have deleterious effects on nanowire device performance. A screening effect was directly observed and found to shift the threshold voltage of the devices by several volts over distances of several microns. The screening effect was established to be present on several different nanowires with differing contact geometries. We believe that the effect should not be limited to InAs and should indeed persist in different material systems. Through simulation, the effect was shown to be a direct result of the relative size of the nanowire compared to the contact and the shape of the probe-tip gate. A reduction in the cross-sectional area of the contact helped quell the simulated screening effect leading us to conclude that an analogous behavior would be seen in experiment. A more conformal gate geometry would ameliorate the effect to some degree, but likely not remove it entirely. These results have implications for the design and expected performance of nanowire-based devices. Moreover, the results highlight the paramount importance of further study of the interaction (whether parasitic or otherwise) between nano- and macro-sized objects in addition to the imperative to take care to design systems that are not debilitated by such effects.

Acknowledgment

We would like to acknowledge the financial support from the Office of Naval Research (ONR-nanoelectronics), and the National Science Foundation (ECS-0506902)

References

[1] Z. Zhong, D. Wang, Y. Cui, M. W. Bockrath, and C. M. Lieber, "Nanowire crossbar arrays as address decoders for integrated nanosystems," *Science* **302**, (2003) pp. 1377.

[2] M. H. Huang, S. Mao, H. Feick, H. Yan, Y. Wu, H. Kind, E. Weber, R. Russo, and P Yang, "Room-temperature ultraviolet nanowire nanolasers," *Science* **292**, (2001) pp. 1897.

[3] F. Patolsky, B. Timko, G. Yu, Y. Fang, A. B. Greytak, G. Zheng, and C. M. Lieber, "Detection, stimulation, and inhibition of neuronal signals with high-density nanowire transistor arrays," *Science* **313**, (2006) pp. 1100.

[4] A I. Boukai, Y. Bunimovich, J Tahir-Kheli, J. Yu, W. A. Goddard III, and J. R. Heath, "Silicon nanowires as efficient thermoelectric materials," *Nature* **451,** (2008) pp. 168.

[5] S. A. Dayeh, E. T. Yu, and D. Wang, "Growth of InAs nanowires on SiO_2 substrates: nucleation, evolution and role of Au nanoparticles," *J. Phys. Chem. C.* **111**, (2007) pp. 13331.

[6] S. A. Dayeh, D. P. R. Aplin, X. Zhou, P. K. L. Yu, E. T. Yu, and D. Wang, "High electron mobility InAs nanowire field-effect transistors," *Small* **3**, (2007) pp. 326.

[7] C. C. Williams, J. Slinkman, W. P. Hough, and H. K. Wickramasinghe, "Lateral dopant profiling with 200 nm resolution by scanning capacitance microscopy," *App. Phys. Lett.* **55**, (1989) pp. 1662.

[8] Y. Huang and C. C. Williams, *J Vac. Sci. Technol. B* **12**, (1994) pp. 369.

[9] D. M. Schaadt, E. J. Miller, E. T. Yu, and J. M. Redwing, "Quantitative analysis of nanoscale electronic properties in an $Al_xGa_{1-x}N$/GaN heterostructure filed-effect transistor," *J. of Vac. Sci. Technol. B* **19** (2001) pp. 1671.

[10] Y. Hu, J. Xiang, G. Liang, H. Yan, and C. M. Lieber, "Sub-100 nanometer channel length Ge/Si nanowire transistors with potential for 2 THz switching speed," *Nano Lett.* **8** no. 3, (2008) pp. 925.

[11] J. Guo, J. Wang, E. Polizzi, S. Datta, and M. Lundstrom, "Electrostatics of Nanowire Transistors," *IEEE Trans. Nanotech.,* **2**, no. 4 (2003) pp. 329.